Hindawi
Shock and Vibration
Volume 2018, Article ID 8385021, 8 pages
https://doi.org/10.1155/2018/8385021

Research Article

Fault Diagnosis of Bearing by Utilizing LWT-SPSR-SVD-Based RVM with Binary Gravitational Search Algorithm

Sheng-wei Fei

College of Mechanical Engineering, Donghua University, Shanghai 201620, China

Correspondence should be addressed to Sheng-wei Fei; fsw@dhu.edu.cn

Received 20 April 2018; Accepted 3 July 2018; Published 2 September 2018

Academic Editor: Adam Glowacz

Copyright © 2018 Sheng-wei Fei. This is an open access article distributed under the Creative Commons Attribution License, which permits unrestricted use, distribution, and reproduction in any medium, provided the original work is properly cited.

The fault diagnosis method of bearing based on lifting wavelet transform (LWT)-self-adaptive phase space reconstruction (SPSR)-singular value decomposition (SVD)-based relevance vector machine (RVM) with binary gravitational search algorithm (BGSA) is presented in this study, among which LWT-SPSR-SVD (LSS) is presented for feature extraction of the bearing vibration signal, the dynamic characteristics of lifting wavelet coefficients' (LWCs') reconstructed signals of the bearing vibration signal can be reflected by SPSR for LWCs' reconstructed signals of the bearing vibration signal, and BGSA is used to select the embedding space dimension and time delay of phase space reconstruction (PSR) and kernel parameter of RVM. In order to show the superiority of LWT-SPSR-SVD-based RVM with BGSA (LSS-BGSA-RVM), the traditional RVM trained by the training samples with the features based on LWT-SVD (LS-RVM) is used to compare with the proposed LSS-BGSA-RVM method. The experimental result demonstrates that compared with LS-RVM, LSS-BGSA-RVM can achieve the higher diagnosis accuracy for bearing.

1. Introduction

Bearing is the important component of mechanical equipment, and the reliable fault diagnosis method of bearing is key to ensuring its safe operation, which is helpful to safe operation of mechanical equipment [1–9]. Support vector machine (SVM) classifier [10–12] has a good ability to solve the classification problems, which has been applied in fault diagnosis of bearing [13]. Relevance vector machine (RVM) based on sparse Bayesian framework has a sparser representation than SVM, which has a better application prospect in fault diagnosis of bearing. However, the selection of the kernel parameter of RVM has a certain influence on its classification performance. Furthermore, the dynamic characteristics of the decomposed signals of the bearing vibration signal should be considered, which can be helpful to obtain the excellent features.

Therefore, in this study, lifting wavelet transform (LWT)-self-adaptive phase space reconstruction (SPSR)-singular value decomposition (SVD)-based RVM with binary gravitational search algorithm (BGSA) is presented and applied for fault diagnosis of bearing, among which LWT-SPSR-SVD (LSS) is presented for feature extraction of the bearing vibration signal. By SPSR for lifting wavelet coefficients' (LWCs') reconstructed signals of the bearing vibration signal, the dynamic characteristics of LWCs' reconstructed signals of the bearing vibration signal can be reflected. SPSR for LWCs' reconstructed signals of the bearing vibration signal can be helpful to obtain the excellent features.

The different embedding space dimension and time delay of phase space reconstruction (PSR) can obtain different PSR signals, which has an influence on the performance of the diagnosis model. Furthermore, the selection of the kernel parameter of RVM has a certain influence on its classification performance. Gravitational search algorithm (GSA) is an intelligent optimization algorithm based on the law of gravity [14–19], and BGSA can be used to solve the optimization problems in the binary space. In BGSA, the heavy masses corresponding to good solutions move more slowly than lighter ones, which can guarantee the algorithm's exploitation step. Thus, BGSA is employed to select the embedding space dimension and time delay of PSR and kernel parameter of RVM. In order to show the superiority

of LWT-SPSR-SVD-based RVM with BGSA (LSS-BGSA-RVM), the traditional RVM trained by the training samples with the features based on LWT-SVD (LS-RVM) is used to compare with the proposed LSS-BGSA-RVM method.

2. Feature Extraction Method of Bearing Vibration Signal Based on LSS

2.1. SPSR for LWCs' Reconstructed Signals of Bearing Vibration Signal. In this study, the bearing vibration signal is decomposed into four LWCs' reconstructed signals with different frequency ranges by performing the three-level decomposition for the bearing vibration signal based on LWT. The different embedding space dimension and time delay of PSR can obtain different PSR signals, which has an influence on the performance of the diagnosis model, so SPSR is used instead of PSR here. By SPSR for LWCs' reconstructed signals of the bearing vibration signal, the dynamic characteristics of LWCs' reconstructed signals of the bearing vibration signal can be reflected. Thus, SPSR for lifting LWCs' reconstructed signals of the bearing vibration signal can be helpful to obtain the excellent features.

Assume that the data set of the rth LWC's reconstructed signal is described as $c_{r,1}, c_{r,2}, \ldots, c_{r,n}$, $(r = 1, 2, 3, 4)$ and define m as embedding space dimension and τ as time delay, the SPSR signal of the rth LWC's reconstructed signal is given as follows:

$$\mathbf{Y}_r = \begin{bmatrix} c_{r,1} & c_{r,2} & \cdots & c_{r,n-(m-1)\times\tau} \\ c_{r,1+\tau} & c_{r,2+\tau} & \cdots & c_{r,n-(m-2)\times\tau} \\ \vdots & \vdots & \ddots & \vdots \\ c_{r,1+(m-1)\times\tau} & c_{r,2+(m-1)\times\tau} & \cdots & c_{r,n} \end{bmatrix}. \quad (1)$$

2.2. SVD for SPSR Signals. SVD [20, 21] for matrix $\mathbf{Y}_r$ which is the SPSR signal of the rth LWC's reconstructed signal can be performed as follows:

$$\mathbf{Y}_r = \mathbf{U}_r \mathbf{S}_r \mathbf{V}_r^T, \quad (2)$$

where $\mathbf{Y}_r$ is a matrix with $m \times [n-(m-1)\times\tau]$; $\mathbf{U}_r$ is an orthogonal matrix with $m \times m$; $\mathbf{V}_r$ is an orthogonal matrix with $[n-(m-1)\times\tau] \times [n-(m-1)\times\tau]$; and $\mathbf{S}_r = [\mathrm{diag}(f_{r,1}, f_{r,2}, \ldots, f_{r,q})\ \mathbf{O}]$, or its transposition, where $\mathbf{O}$ is the zero matrix, $q = \min\{m, n-(m-1)\times\tau\}$, and $f_{r,1}, f_{r,2}, \ldots, f_{r,q}$ are the singular values of the matrix $\mathbf{Y}_r$, $f_{r,\delta} \geq 0$, $(r = 1, 2, 3, 4;\ \delta = 1, 2, \ldots, q)$.

2.3. Obtaining the Features of Bearing Vibration Signal Based on LSS. The singular values of the SPSR signals of the four LWCs' reconstructed signals of the bearing vibration signal constitute a vector as $[f_{1,1} \cdots f_{1,q}\ f_{2,1} \cdots f_{2,q}\ f_{3,1} \cdots f_{3,q}\ f_{4,1} \cdots f_{4,q}]$. Calculate the relative values of the elements in the vector as follows:

$$\widehat{f}_{r,\delta} = \frac{f_{r,\delta}}{\sum_{r=1}^{4}\sum_{\delta=1}^{q} f_{r,\delta}}. \quad (3)$$

Thus, the features of the bearing vibration signal based on LSS are described as $[\widehat{f}_{1,1} \cdots \widehat{f}_{1,q}\ \widehat{f}_{2,1} \cdots \widehat{f}_{2,q}\ \widehat{f}_{3,1} \cdots \widehat{f}_{3,q}\ \widehat{f}_{4,1} \cdots \widehat{f}_{4,q}]$.

When m is less than or equal to $n-(m-1)\times\tau$, the features of the bearing vibration signal based on LSS can be described as $[\widehat{f}_{1,1} \cdots \widehat{f}_{1,m}\ \widehat{f}_{2,1} \cdots \widehat{f}_{2,m}\ \widehat{f}_{3,1} \cdots \widehat{f}_{3,m}\ \widehat{f}_{4,1} \cdots \widehat{f}_{4,m}]$.

3. RVM Classifier

Given a set of training samples $\mathbf{E} = (\mathbf{Z}, \mathbf{H})$, the likelihood function obeys the Bernoulli distribution [22]:

$$P(\mathbf{H}|\mathbf{Z}) = \prod_{b=1}^{N} \sigma\{y(\mathbf{z}_b;\ \mathbf{W})\}^{h_b} [1-\sigma\{y(\mathbf{z}_b;\ \mathbf{W})\}]^{1-h_b}, \quad (4)$$

where $\mathbf{Z} = \{\mathbf{z}_b\}_{b=1}^{N}$, $\mathbf{z}_b$ denotes the input vector; $\mathbf{H} = \{h_b\}_{b=1}^{N}$, h_b denotes the corresponding output target, $h_b \in \{0, 1\}$, "0" and "1" denote two classes which the training samples belong to; and N denotes the number of training samples; $\sigma\{y(\mathbf{z}_b;\ \mathbf{W})\}$ is a predefined logistic sigmoid function, $\sigma\{y(\mathbf{z}_b;\ \mathbf{W})\} = 1/(1+e^{-y(\mathbf{z}_b;\mathbf{W})})$; and $\mathbf{W}$ is the weight vector.

Here, radial basis function (RBF) kernel can be described as the following equation, which can be used to construct the RVM,

$$K(\mathbf{z}_b,\ \mathbf{z}) = \exp\left(-p\left\|\mathbf{z}_b - \mathbf{z}\right\|^2\right), \quad (5)$$

where $p\,(p > 0)$ denotes the RBF kernel parameter.

4. Optimizing the Embedding Space Dimension and Time Delay of PSR and Kernel Parameter of RVM Based on BGSA

In this study, BGSA is used to select m (embedding space dimension) and τ (time delay) of PSR and p (kernel parameter) of RVM. In BGSA, solutions are encoded as binary vectors; agents can be considered as objects, and their performance can be measured by their masses [23]. Figure 1 shows the process of the selection of m (embedding space dimension) and τ (time delay) of PSR and p (kernel parameter) of RVM by BGSA, which can be described in detail as follows:

Step 1. Encode m (embedding space dimension) and τ (time delay) of PSR and p (kernel parameter) of RVM, and randomly initialize the positions of B agents in the search space. The position of the ith agent is defined by the following vector:

$$\mathbf{x}_i = \left(x_i^1, \ldots, x_i^d, \ldots, x_i^D\right), \quad i = 1, 2, \ldots, B, \quad (6)$$

where x_i^d denotes the position of the ith agent in the dth dimension and B denotes the number of the agents.

As shown in Table 1, the first part of binary code string represents the embedding space dimension m of PSR and l denotes the length of binary code string representing the embedding space dimension m of PSR. The second part of binary code string represents the time delay τ of PSR, and u denotes the length of binary code string representing the time delay τ of PSR. The third part of binary code string

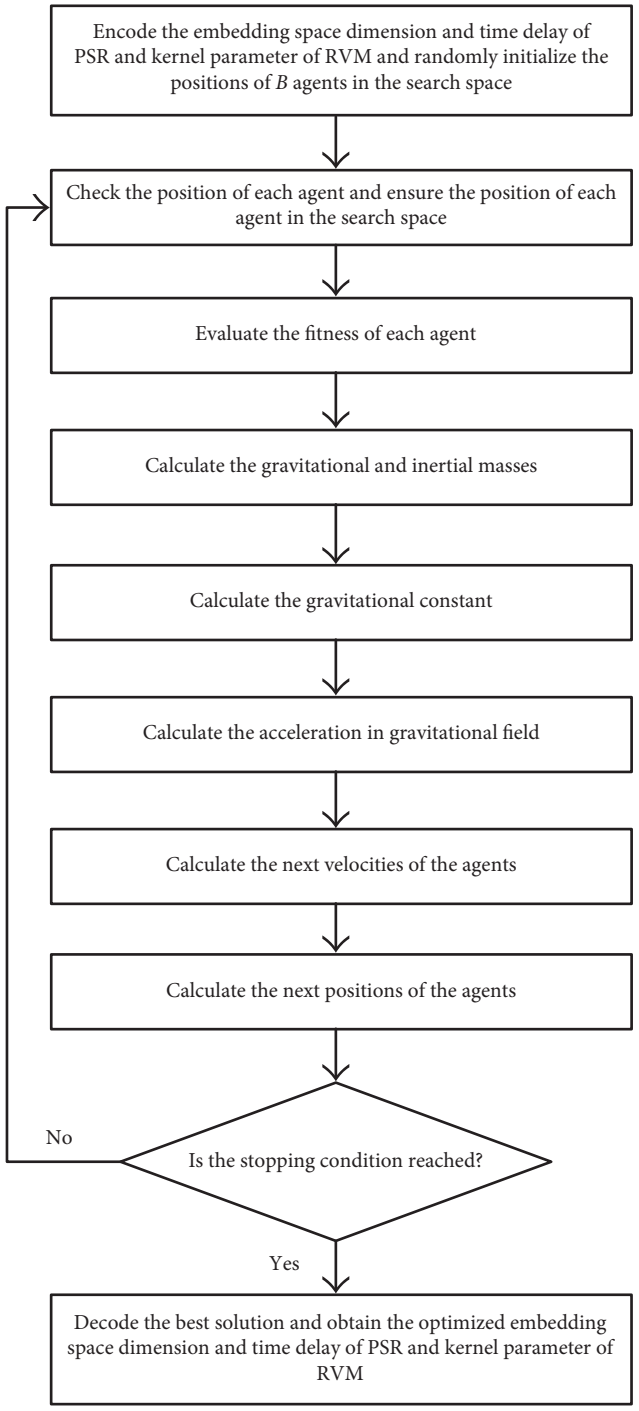

Figure 1: The process of the selection of m (embedding space dimension) and τ (time delay) of PSR and p (kernel parameter) of RVM by BGSA.

represents the kernel parameter p of RVM, and $L-(l+u)$ denotes the length of the binary code string representing the kernel parameter p of RVM.

Step 2. Check the position of each agent, and ensure the position of each agent in the search space. Check the binary codes representing the embedding space dimension m of PSR, the binary codes representing the time delay τ of PSR, and the binary codes representing the kernel parameter p of RVM of each agent, and ensure that the decimal value of the binary codes representing the embedding space dimension m of each agent is 2 at least, one of the binary codes representing the time delay τ of each agent is "1" at least, and one of the binary codes representing the kernel parameter p of each agent is "1" at least.

Table 1: Encoding m (embedding space dimension) and τ (time delay) of PSR and p (kernel parameter) of RVM.

m			τ			p		
x_i^1	...	x_i^l	x_i^{l+1}	...	x_i^{l+u}	x_i^{l+u+1}	...	x_i^L

Step 3. Evaluate the Fitness of Each Agent. The training samples are divided equally into Q subsets of the samples, among which $Q-1$ subsets of the samples are employed to train the RVM model, and the remaining subset is used to test the RVM model. Each subset can be employed as the testing subset. Then, the total diagnosis accuracy A_i of the Q subsets of the samples can be obtained as follows:

$$A_i = \frac{N_{\text{correct}}}{N_{\text{total}}}, \tag{7}$$

where N_{total} denotes the total number of the Q subsets of the samples, N_{correct} denotes the total number of the Q subsets of the samples with correct diagnosis, and Q is set to 5 here.

Here, the fitness of the ith agent is defined as follows:

$$\text{fit}_i = 1 - A_i. \tag{8}$$

Step 4. The gravitational and inertial masses can be calculated as follows:

$$\begin{aligned} m_i(t) &= \frac{\text{fit}_i(t) - \text{worst}(t)}{\text{best}(t) - \text{worst}(t)}, \\ M_i(t) &= \frac{m_i(t)}{\sum_{j=1}^{B} m_j(t)}, \end{aligned} \tag{9}$$

where $t = 1, 2, \ldots, T$ (T denotes the total number of iterations), $\text{fit}_i(t)$ denotes the fitness value of the ith agent at iteration t, and for a minimization problem, $\text{best}(t)$ and $\text{worst}(t)$ are, respectively, defined as follows:

$$\begin{aligned} \text{best}(t) &= \min_{j\in\{1,\ldots,B\}} \text{fit}_j(t), \\ \text{worst}(t) &= \max_{j\in\{1,\ldots,B\}} \text{fit}_j(t). \end{aligned} \tag{10}$$

Step 5. The gravitational constant can be calculated as follows:

$$G(t) = G_0 \times \exp\left(-\frac{\lambda \times t}{T}\right), \tag{11}$$

where G_0 and λ are the constants.

Step 6. Calculate the Acceleration in Gravitational Field. First, the force acting on mass "i" from mass "j" can be calculated as follows:

$$F_{ij}^{d}(t) = G(t)\frac{M_{pi}(t) \times M_{aj}(t)}{R_{ij}(t) + \varepsilon}\left(x_j^d(t) - x_i^d(t)\right), \quad (12)$$

where $G(t)$ denotes gravitational constant at iteration t, $M_{pi}(t)$ denotes the passive gravitational mass related to the ith agent, $M_{aj}(t)$ denotes the active gravitational mass related to the jth agent, ε denotes a small constant, and $R_{ij}(t)$ denotes the Euclidian distance between two agents i and j:

$$R_{ij}(t) = \left\|\mathbf{x}_i(t),\ \mathbf{x}_j(t)\right\|_2. \quad (13)$$

Kbest is an iteration function, which is expressed as follows:

$$Kbest = \text{round}\left(B \times \frac{K_0 + (1 - ((t-1)/(T-1))) \times (100 - K_0)}{100}\right),$$

Subject to

$$\text{round}\left(\frac{B \times K_0}{100}\right) = 1, \quad (14)$$

where the function round is used to be rounded to the nearest integer number here and K_0 is the constant.

Then,

$$F_i^d(t) = \sum_{j=1, i\neq j}^{Kbest} \text{rand}_j F_{ij}^d(t), \quad (15)$$

where rand_j is a random number in the range of 0~1.

By the law of motion, $a_i^d(t)$ which is the acceleration of the ith agent at iteration t in the dth direction can be given as follows:

$$a_i^d(t) = \frac{F_i^d(t)}{M_{ii}(t)}, \quad (16)$$

where M_{ii} is the inertial mass of the ith agent.

As $M_{pi} = M_{ai} = M_{ii} = M_i$, $a_i^d(t)$ can be given as follows:

$$a_i^d(t) = \sum_{j=1, i\neq j}^{Kbest} \text{rand}_j\left[G(t)\frac{M_j(t)}{R_{ij}(t) + \varepsilon}\left(x_j^d(t) - x_i^d(t)\right)\right]. \quad (17)$$

Step 7. Calculate the Next Velocities of the Agents. The next velocity of an agent can be calculated as follows:

$$v_i^d(t+1) = \text{rand}_i \times v_i^d(t) + a_i^d(t), \quad (18)$$

where rand_i is a uniform random variable in the range of 0~1, $v_i^d(t+1)$ denotes the ith agent's velocity at the $(t+1)$th iteration in the dth dimension, and the maximum value of $|v_i^d(t+1)|$ is set to 6 here.

Step 8. Calculate the Next Positions of the Agents. The next position of an agent can be calculated as follows:

$$VT\left(v_i^d(t+1)\right) = \left|\tanh\left(v_i^d(t+1)\right)\right|,$$
$$x_i^d(t+1) = \begin{cases} \widetilde{x}_i^d(t), & \text{rand} < VT\left(v_i^d(t+1)\right), \\ x_i^d(t), & \text{rand} \geq VT\left(v_i^d(t+1)\right), \end{cases} \quad (19)$$

where $x_i^d(t+1)$ denotes the ith agent's position at the $(t+1)$th iteration in the dth dimension, $\widetilde{x}_i^d(t)$ denotes the complement of $x_i^d(t)$, and rand denotes a random value in the range of 0~1.

Step 9. Repeat Step 2 to Step 8 until the stopping condition is reached.

Step 10. Decode the best solution, and the optimized m (embedding space dimension) and τ (time delay) of PSR and p (kernel parameter) of RVM can be obtained.

5. Experimental Analysis

In the experiment, the bearing vibration data are obtained from "bearings vibration data set" of Case Western Reserve University, among which the fault data are collected under the condition of single point faults with a fault diameter of 0.014 inches [24]. Three groups of samples are derived from bearing vibration signals acquired under three different loads. In group 1, the samples are obtained based on the bearing vibration signal acquired under 1 HP motor load. In group 2, the samples are obtained based on the bearing vibration signal acquired under 2 HP motor load. In group 3, the samples are obtained based on the bearing vibration signal acquired under 3 HP motor load. Each group includes 200 samples, among which 50 samples represent normal state, 50 samples represent inner race fault, 50 samples represent outer race fault, and 50 samples represent ball fault.

The first 40 samples of each state in each group are employed as the training samples, and the remaining 10 samples of each state in each group are employed as the testing samples. Thus, the training samples include 480 samples, and the testing samples include 120 samples.

Four LWCs' reconstructed signals of the bearing vibration signal are obtained by performing the three-level decomposition for the bearing vibration signal based on LWT. Figure 2 gives the four LWCs' reconstructed signals of one of the samples representing the normal state in the training samples.

In the proposed LSS-BGSA-RVM method, the features of the bearing vibration signal are obtained by using the feature extraction method of the bearing vibration signal based on LSS, and BGSA is used to select m (embedding space dimension) and τ (time delay) of PSR and p (kernel parameter) of RVM. The value range of the embedding space dimension m of PSR is [2, 2^3−1], and the intervals of the adjacent values of the embedding space dimension m are 1; thus, the length of binary code string representing the embedding space dimension m is 3. The value range of the time delay τ of PSR is [1, 2^3−1], and the intervals of the

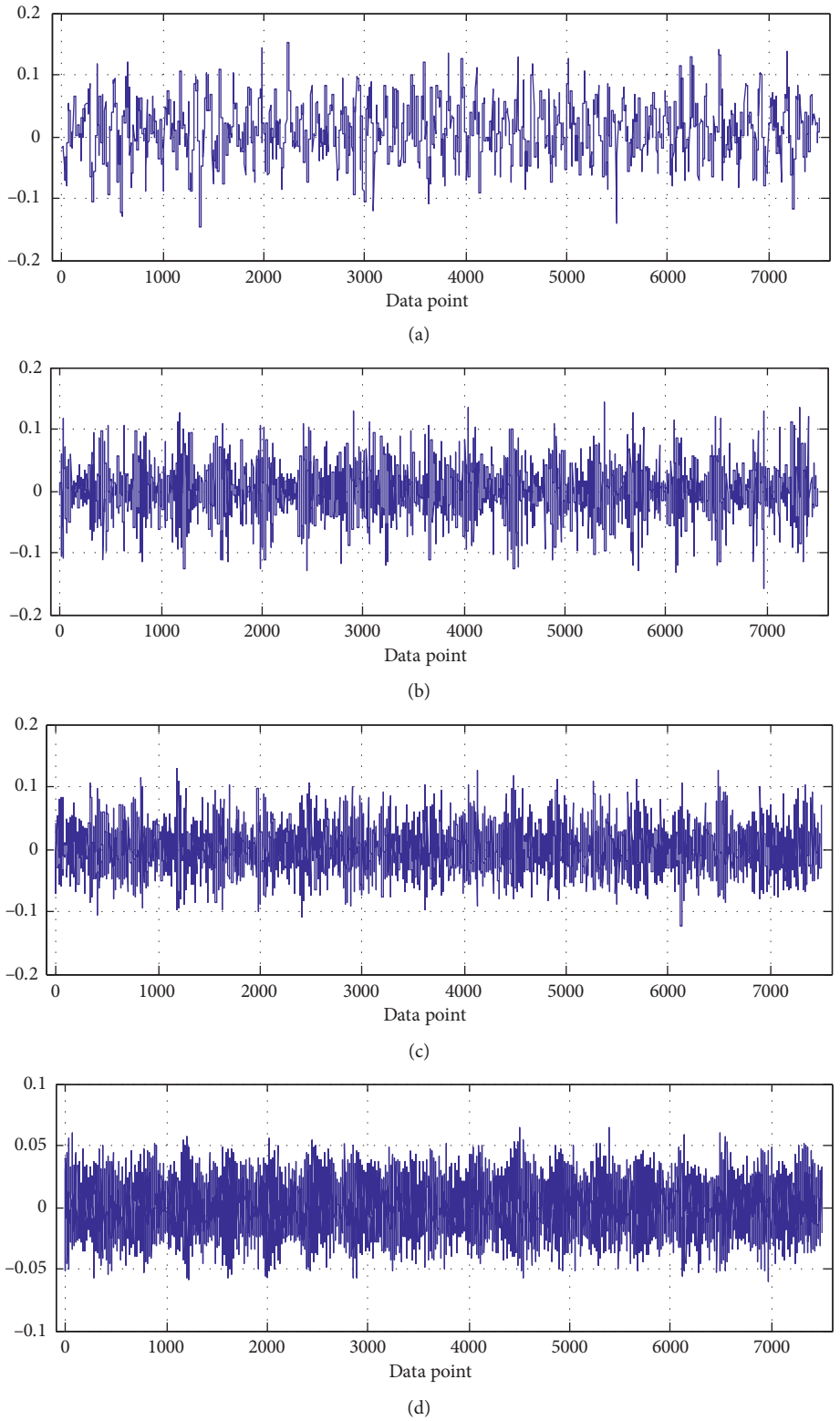

Figure 2: The four LWCs' reconstructed signals of one of the samples representing the normal state in the training samples. (a) Reconstructed signal of lifting wavelet coefficient 1, (b) reconstructed signal of lifting wavelet coefficient 2, (c) reconstructed signal of lifting wavelet coefficient 3, and (d) reconstructed signal of lifting wavelet coefficient 4.

adjacent values of the time delay τ are 1; thus, the length of binary code string representing the time delay τ is 3. The value range of the kernel parameter p is $[1, 2^{10}-1]$, and the intervals of the adjacent values of the kernel parameter p are 1; thus, the length of binary code string representing the kernel parameter p is 10. Obviously, in this case,

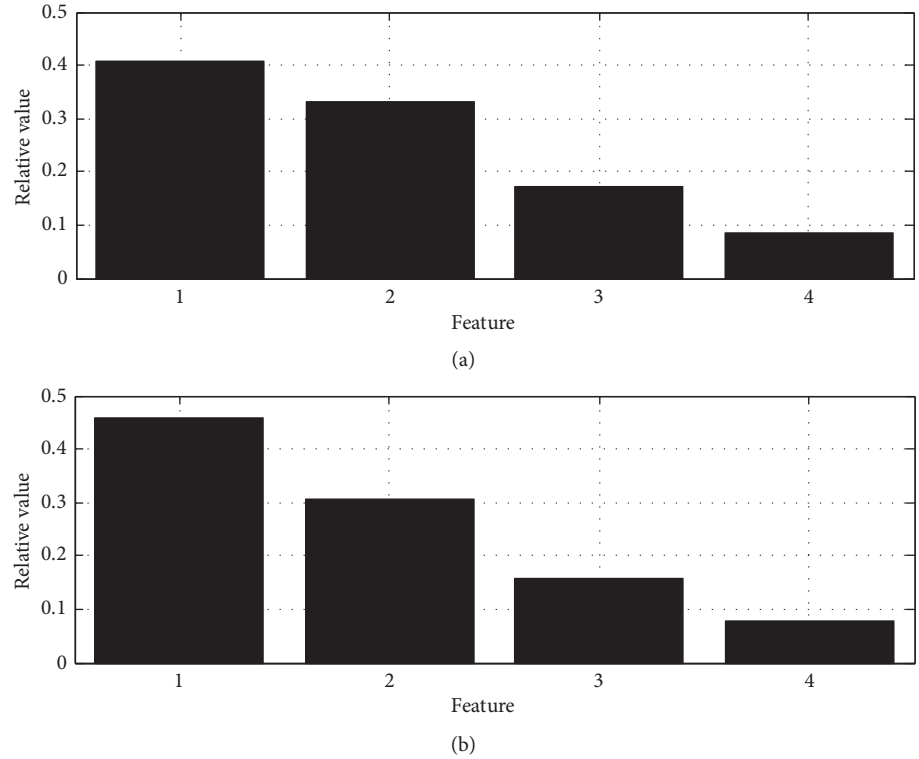

Figure 3: The features of two samples representing outer race fault and ball fault, respectively, in a set of samples based on LWT-SVD. (a) The features of the sample representing outer race fault, and (b) the features of the sample representing ball fault.

$[n-(m-1)\times\tau]>m$, so the features of the bearing vibration signal based on LSS can be described as $[\widehat{f}_{1,1}\cdots\widehat{f}_{1,m}\ \widehat{f}_{2,1}\cdots\widehat{f}_{2,m}\ \widehat{f}_{3,1}\cdots\widehat{f}_{3,m}\ \widehat{f}_{4,1}\cdots\widehat{f}_{4,m}]$ here. Then, the diagnosis model of bearing is established by three LSS-BGSA-RVMs with the form of binary tree, among which LSS-BGSA-RVM1 is employed to separate the normal state from the fault state, LSS-BGSA-RVM2 is employed to separate inner race fault from other faults (outer race fault and ball fault), and LSS-BGSA-RVM3 is employed to separate outer race fault from ball fault. The values of the respective embedding space dimensions, time delays, and kernel parameters of LSS-BGSA-RVM1, LSS-BGSA-RVM2, and LSS-BGSA-RVM3 can be obtained by BGSA.

In order to show the superiority of the proposed LSS-BGSA-RVM method, the LS-RVM method is used to compare with the proposed LSS-BGSA-RVM method. In the LS-RVM method, the features of the bearing vibration signal are obtained by using the feature extraction method of the bearing vibration signal based on LWT-SVD. Define $g_1, g_2, \ldots, g_\beta$ as the singular values of the matrix $\mathbf{C}$ which is composed of the four LWCs' reconstructed signals of the bearing vibration signal,

$$\mathbf{C}=\begin{bmatrix} c_{1,1} & c_{1,2} & \cdots & c_{1,n} \\ c_{2,1} & c_{2,2} & \cdots & c_{2,n} \\ c_{3,1} & c_{3,2} & \cdots & c_{3,n} \\ c_{4,1} & c_{4,1} & \cdots & c_{4,n} \end{bmatrix}, \quad \beta=\min\{4,\ n\}, \quad g_\rho\geq 0, \tag{20}$$

($\rho=1,\ 2,\ \ldots,\ \beta$), and the singular values of the matrix composed of the four LWCs' reconstructed signals of the bearing vibration signal constitute a vector as $[g_1\ g_2\ \ldots\ g_\beta]$. Calculate the relative values of the elements in the vector as follows:

$$\widehat{g}_\rho=\frac{g_\rho}{\sum_{\rho=1}^{\beta}g_\rho}. \tag{21}$$

Thus, the features of the bearing vibration signal based on LWT-SVD are described as $[\widehat{g}_1\ \widehat{g}_2\ \ldots\ \widehat{g}_\beta]$. Obviously, in this case, $n>4$, so the features of the bearing vibration signal based on LWT-SVD can be described as $[\widehat{g}_1\ \widehat{g}_2\ \widehat{g}_3\ \widehat{g}_4]$ here. Moreover, in the LS-RVM method, the grid method is used to select the kernel parameter p of RVM; here, the value range of the kernel parameter p is $[1, 2^{10}-1]$, and the intervals of the adjacent values of the kernel parameter p are 1. Then, the diagnosis model of bearing is established by three LS-RVMs with the form of binary tree, among which LS-RVM1 is employed to separate the normal state from the fault state, LS-RVM2 is employed to separate inner race fault from other faults (outer race fault and ball fault), and LS-RVM3 is employed to separate outer race fault from ball fault. The values of the respective kernel parameters of LS-RVM1, LS-RVM2, and LS-RVM3 can be obtained by the grid method.

The diagnosis accuracy (DA) described in the following equation is used to evaluate the performance of the diagnosis models,

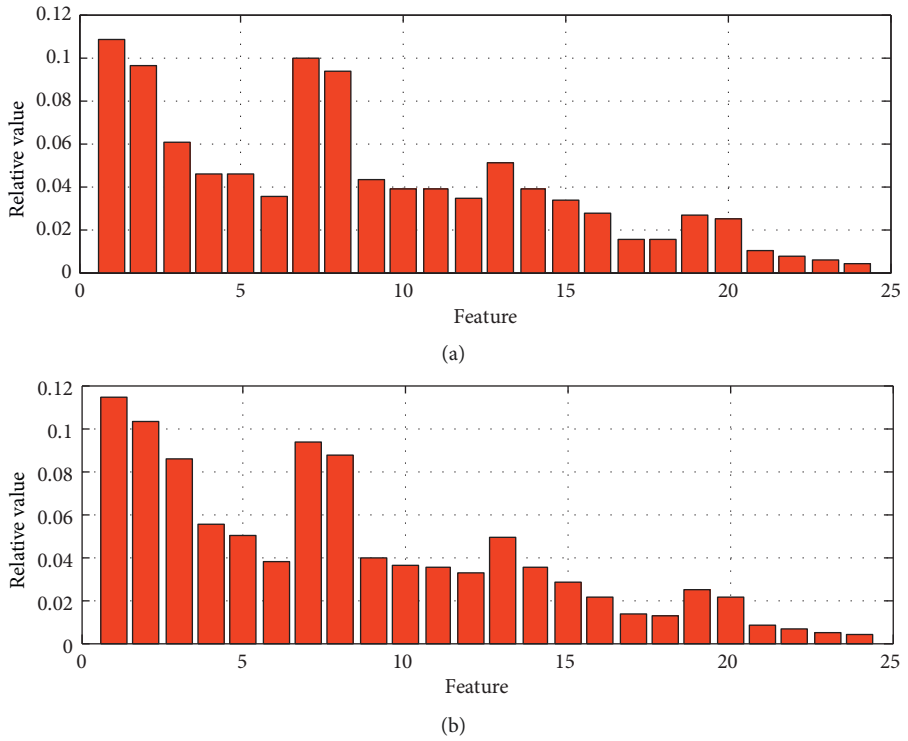

Figure 4: The features of two samples representing outer race fault and ball fault, respectively, in a set of samples based on LSS in LSS-BGSA-RVM3. (a) The features of the sample representing outer race fault, and (b) the features of the sample representing ball fault.

Table 2: The comparison of the diagnosis accuracy of bearing between LSS-BGSA-RVM and LS-RVM.

The number of the testing samples	Classifier	The number of the testing samples with correct diagnosis	Diagnosis accuracy (%)
120	LSS-BGSA-RVM	119	99.17
	LS-RVM	108	90

$$\mathrm{DA} = \frac{\Phi_{\mathrm{correct}}}{\Phi_{\mathrm{total}}} \times 100\%, \tag{22}$$

where Φ_{total} is the number of testing samples and Φ_{correct} is the number of testing samples with correct diagnosis in the case.

The features of two samples representing outer race fault and ball fault, respectively, in a set of samples based on LWT-SVD can be shown in Figure 3, and for the same samples as above, their features based on LSS in LSS-BGSA-RVM3 can be shown in Figure 4. As in shown in Table 2, only one testing sample is incorrectly diagnosed by using LSS-BGSA-RVM, and 119 testing samples are correctly diagnosed by using LSS-BGSA-RVM; then, the diagnosis accuracy of bearing by using LSS-BGSA-RVM is 99.17%. However, 12 testing samples are incorrectly diagnosed by using LS-RVM, and 108 testing samples are correctly diagnosed by using LS-RVM; then, the diagnosis accuracy of bearing by using LS-RVM is 90%. The experimental result demonstrates that LSS-BGSA-RVM can achieve the higher diagnosis accuracy of bearing than LS-RVM, and the proposed LSS-BGSA-RVM method for fault diagnosis of bearing is feasible.

6. Conclusion

In this study, the fault diagnosis method of bearing based on LSS-based RVM with BGSA is presented, among which LSS is presented for feature extraction of the bearing vibration signal, and BGSA is used to select the embedding space dimension and time delay of PSR and kernel parameter of RVM. BGSA can be used to solve the optimization problems in the binary space. In BGSA, the heavy masses corresponding to good solutions move more slowly than lighter ones, which can guarantee the algorithm's exploitation step. By SPSR for LWCs' reconstructed signals of the bearing vibration signal, the dynamic characteristics of LWCs' reconstructed signals of the bearing vibration signal can be reflected. SPSR for LWCs' reconstructed signals of the bearing vibration signal can be helpful to obtain the excellent features. The experimental result demonstrates that compared with LS-RVM, LSS-BGSA-RVM can achieve the higher diagnosis accuracy for bearing.

Data Availability

The data used to support the findings of this study are available from the corresponding author upon request.

Conflicts of Interest

The author confirms that there are no conflicts of interest.

Acknowledgments

This project is supported by the "Fundamental Research Funds for the Central Universities (no. 2232017D-14)."

References

[1] Y. B. Li, M. Q. Xu, X. H. Liang, and W. H. Huang, "Application of bandwidth EMD and adaptive multiscale morphology analysis for incipient fault diagnosis of rolling bearings," *IEEE Transactions on Industrial Electronics*, vol. 64, no. 8, pp. 6506–6517, 2017.

[2] A. Glowacz, W. Glowacz, Z. Glowacz, and J. Kozik, "Early fault diagnosis of bearing and stator faults of the single-phase induction motor using acoustic signals," *Measurement*, vol. 113, pp. 1–9, 2018.

[3] A. Medoued, M. Mordjaoui, Y. Soufi, and D. Sayad, "Induction machine bearing fault diagnosis based on the axial vibration analytic signal," *International Journal of Hydrogen Energy*, vol. 41, no. 29, pp. 12688–12695, 2016.

[4] J. M. Li, M. Li, and J. F. Zhang, "Rolling bearing fault diagnosis based on time-delayed feedback monostable stochastic resonance and adaptive minimum entropy deconvolution," *Journal of Sound and Vibration*, vol. 401, pp. 139–151, 2017.

[5] S. B. Wang, I. Selesnick, G. G. Cai, Y. N. Feng, X. Sui, and X. F. Chen, "Nonconvex sparse regularization and convex optimization for bearing fault diagnosis," *IEEE Transactions on Industrial Electronics*, vol. 65, no. 9, pp. 7332–7342, 2018.

[6] F. Dalvand, S. Dalvand, F. Sharafi, and M. Pecht, "Current noise cancellation for bearing fault diagnosis using time shifting," *IEEE Transactions on Industrial Electronics*, vol. 64, no. 10, pp. 8138–8147, 2017.

[7] S. L. Lu, Q. B. He, T. Yuan, and F. R. Kong, "Online fault diagnosis of motor bearing via stochastic-resonance-based adaptive filter in an embedded system," *IEEE Transactions on Systems, Man, and Cybernetics: Systems*, vol. 47, no. 7, pp. 1111–1122, 2017.

[8] C. P. Mbo'o and K. Hameyer, "Fault diagnosis of bearing damage by means of the linear discriminant analysis of stator current features from the frequency selection," *IEEE Transactions on Industry Applications*, vol. 52, no. 5, pp. 3861–3868, 2016.

[9] M. He, D. He, and Y. Z. Qu, "A new signal processing and feature extraction approach for bearing fault diagnosis using AE sensors," *Journal of Failure Analysis and Prevention*, vol. 16, no. 5, pp. 821–827, 2016.

[10] H. W. Wang, J. Gu, and S. S. Wang, "An effective intrusion detection framework based on SVM with feature augmentation," *Knowledge-Based Systems*, vol. 136, pp. 130–139, 2017.

[11] S. Liu and M. Whitty, "Automatic grape bunch detection in vineyards with an SVM classifier," *Journal of Applied Logic*, vol. 13, no. 4, pp. 643–653, 2015.

[12] C. Singh, E. Walia, and K. P. Kaur, "Enhancing color image retrieval performance with feature fusion and non-linear support vector machine classifier," *Optik*, vol. 158, pp. 127–141, 2018.

[13] S. E. Pandarakone, Y. Mizuno, and H. Nakamura, "Distinct fault analysis of induction motor bearing using frequency spectrum determination and support vector machine," *IEEE Transactions on Industry Applications*, vol. 53, no. 3, pp. 3049–3056, 2017.

[14] A. Bahrololoum, H. Nezamabadi-pour, H. Bahrololoum, and M. Saeed, "A prototype classifier based on gravitational search algorithm," *Applied Soft Computing*, vol. 12, no. 2, pp. 819–825, 2012.

[15] E. Rashedi, H. Nezamabadi-pour, and S. Saryazdi, "GSA: a gravitational search algorithm," *Information Sciences*, vol. 179, no. 13, pp. 2232–2248, 2009.

[16] P. K. Roy, "Solution of unit commitment problem using gravitational search algorithm," *International Journal of Electrical Power & Energy Systems*, vol. 53, pp. 85–94, 2013.

[17] V. Kumar, J. K. Chhabra, and D. Kumar, "Automatic cluster evolution using gravitational search algorithm and its application on image segmentation," *Engineering Applications of Artificial Intelligence*, vol. 29, pp. 93–103, 2014.

[18] S. D. Beigvand, H. Abdi, and M. La Scala, "Combined heat and power economic dispatch problem using gravitational search algorithm," *Electric Power Systems Research*, vol. 133, pp. 160–172, 2016.

[19] G. S. Grewal and B. Singh, "Efficiency determination of in-service induction machines using gravitational search optimization," *Measurement*, vol. 118, pp. 156–163, 2018.

[20] P. K. Dhar and T. Shimamura, "Audio watermarking in transform domain based on singular value decomposition and Cartesian-polar transformation," *International Journal of Speech Technology*, vol. 17, no. 2, pp. 133–144, 2014.

[21] A. R. Elshazly, M. E. Nasr, M. M. Fouad, and F. S. Abdel-Samie, "High payload multi-channel dual audio watermarking algorithm based on discrete wavelet transform and singular value decomposition," *International Journal of Speech Technology*, vol. 20, no. 4, pp. 951–958, 2017.

[22] M. E. Tipping, "Sparse Bayesian learning and the relevance vector machine," *Journal of Machine Learning Research*, vol. 1, pp. 211–244, 2001.

[23] E. Rashedi, H. Nezamabadi-pour, and S. Saryazdi, "BGSA: binary gravitational search algorithm," *Natural Computing*, vol. 9, no. 3, pp. 727–745, 2010.

[24] K. A. Loparo, *Bearings Vibration Data Set*, Case Western Reserve University, Cleveland, OH, USA, 2003.

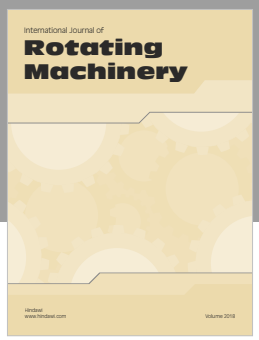

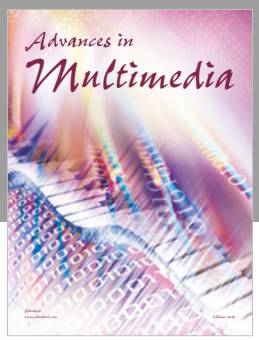

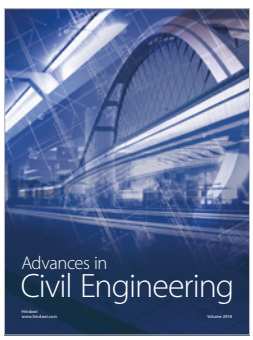

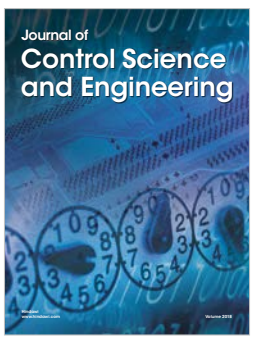

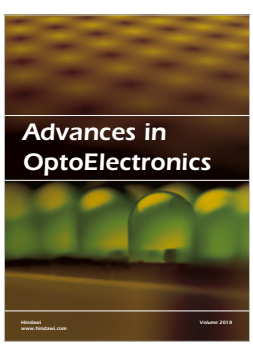

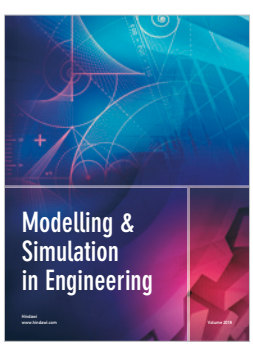

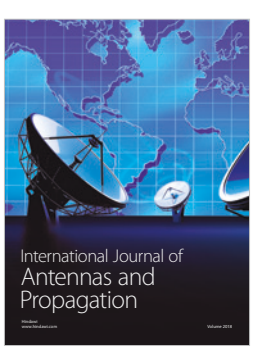

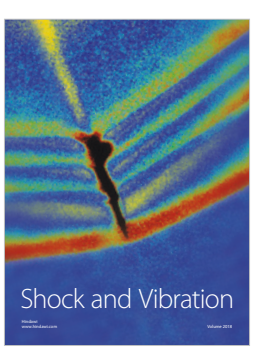

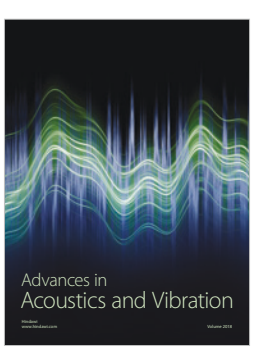

Hindawi

Submit your manuscripts at
www.hindawi.com